EVALUATION OF A NON-COHERENT SYNTHETIC APERTURE SONAR AUTOFOCUS

VL Myers Defence R&D Canada, Dartmouth, Nova Scotia, Canada
DP Williams Defence Science and Technology Laboratory, Porton Down, UK
J Dillon Kraken Robotics, St. John's, NL, Canada

1 INTRODUCTION

One of the main challenges of practical high-frequency (HF) Synthetic Aperture Sonar (SAS) systems in creating well-focused images lies in estimating and correcting for the deviations of the host platform, usually an unmanned underwater vehicle (UUV), from an ideal linear track. These need to be determined to a precision on the order of one-tenth of a wavelength — fractions of millimetres for the frequencies considered in this paper. Commonly used techniques such as the Displaced Phase Centre Antenna (DPCA) [6] micronavigation method use time-delay estimation between overlapping pings to determine precise (relative) inter-ping sway and surge displacements that are used to correct the array transducer positions. These techniques are typically aided by using high-grade Inertial Navigation Systems (INS) to estimate the heading, which is the main limiting factor in the accuracy of the DPCA method. In SAS, DPCA can only be applied if there is signal coherence between two overlapping phase centres on successive pings.

There are cases, however, when the ping-to-ping coherence obtained from the seabed is poor, for instance if there are large areas of shadows or when the seabed does not scatter a great deal of energy back towards the receiver. In these cases, alternative reconstruction methods to produce focused imagery are needed. Another potential application for alternative methods is when one wishes to exceed the restrictions placed on the ping-to-ping displacement of the sonar, which is half the length of the real aperture when using DPCA, in order to increase the rate of coverage of the system. This paper considers SAS image reconstruction in the case when there is little to no ping-to-ping coherence by examining alternatives to the DPCA method. To do this, a SAS system was re-positioned in an upward fashion and directed towards the surface. Since the sea surface is not expected to be coherent from ping to ping, the DPCA method would not be expected to provide acceptable performance and is used as a surrogate for a poor seabed situation. The data is used in this paper to test a new autofocus method which attempts to maximize the sharpness of the SAS image. Results for both downward (seabed) facing and upward (surface) facing SAS show improved image quality of the objects present in the SAS data using the proposed autofocus method.

2 AUTOFOCUS USING SHARPNESS OPTIMIZATION

For most high-frequency SAS systems, coarse motion compensation using inertial sensors is not precise enough to produce sharp, focused imagery and therefore nearly all practical SAS implementations employ some kind of fine motion compensation method, with the DPCA method being the most widely used [15]. The use of a single transmitter coupled with a linear Vernier array composed of m hydrophone elements of size d for a total length of $L = m \times d$ [11] form the basis of the DPCA method, which performs time-delay estimation using the complex cross-correlation of successive pings to determine the navigation correction required to correct for non-linearities in the synthetic array. As long as along-track sampling requirements are satisfied, then there will be at least two overlapping phase centres that can be used for motion estimation. The function $f_{\mathrm{DPCA}}(p, p+1) = [k_x, \tau]$ returns the along-track lag k_x in number of elements that provide the maximum coherence between pings p and $p+1$ as well as an estimate of the time delay between them. The ping-to-ping surge (longitudinal to the direction of travel of the platform) is

then computed as:

$$\delta_p = k_x \times d/2, \tag{1}$$

and the ping-to-ping sway (transverse to the motion of the platform) is:

$$\rho_p = \tau \times c/2. \tag{2}$$

where c is the speed of sound in water. The ping-to-ping yaw [12] can also be estimated using the DPCA method, however its precision is limited by the number of overlapping phase centres, and in most cases if a high-grade INS is present then the INS yaw estimate is used [1]. The image reconstruction process uses the estimated sway, surge and yaw values at each ping to determine the appropriate time delay which must be applied to the returned data at each of the image focal points. The *van Cittert-Zernicke* theorem [2] enables this approach when imaging the seafloor. Under most SAS imaging conditions, the stationary scatterers on the seabed will demonstrate a high degree of coherence from ping-to-ping. This is not always the case for seabed returns and in such situations, other SAS reconstruction methods are needed. An extreme example of this case can be tested by pointing the SAS at the surface which is in principle non-stationary.

DPCA is a type of autofocus, using the acoustic returns to estimate motion in order to form the SAS image. Autofocus algorithms fall into two general categories: Parametric and Non-parametric. In a Parametric approach, the phase error is assumed to follow some general form, for instance quadratic in nature. Sound speed errors can be modelled as a quadratic phase error which will manifest itself as a blurring of the image. A good treatment of stripmap phase errors can be found in [5]. Non-parametric or statistical approaches use the sonar data itself to estimate the phase error, typically maximizing some quality metric such as sharpness:

$$\mathcal{Q}_{\,\mathrm{sharp}} = \sum_{x,y} I(x,y)^2, \tag{3}$$

or contrast:

$$\mathcal{Q}_{\,\mathrm{cst}} = \frac{1}{NM} \sum_{x,y} \frac{\sigma}{\mu}, \tag{4}$$

where

$$\mu = \frac{1}{NM} \sum_{x,y} I(x,y), \tag{5}$$

and

$$\sigma = \sqrt{\frac{1}{NM} \sum_{x,y} (I(x,y) - \mu)^2}, \tag{6}$$

and $I(x,y)$ is the complex modulus of the M by N SAS image. Gradient descent algorithms can be used to maximize any quality metric for which a gradient has been derived, and both the SAS and SAR literature are rich with examples [8, 14, 7, 13, 1]. Well-established algorithms from the SAR community for spotlight-mode autofocus algorithms such as the Phase Difference Autofocus (PDA) [4] and Phase Gradient Autofocus [17] have been extended to stripmap-mode SAS [3]. These techniques rely on strong point scatterers to estimate residual sway errors until a threshold is reached.

2.1 Sway estimation using a sharpness criterion

The most important component of the motion solution after yaw is the ping-to-ping sway ρ. A method was implemented to search for the value of ρ_p over n pings such that the image sharpness criteria $\mathcal{Q}_{\,\mathrm{sharp}}$ is maximized. Initial attempts using the contrast criterion $\mathcal{Q}_{\,\mathrm{cst}}$ found that the sharpness metric resulted in better focused images. Also, since this is a fine motion compensation method (vice a pure autofocus technique), a gradient descent method did not give satisfactory results: this is due to the fact that the sharpness function has many local maxima and unless one can bound the search to within a single resolution cell is unlikely to yield satisfactory results.

[1] There are many challenges and techniques in a practical micronavigation system implementation, including beamforming, interpolation, phase unwrapping and navigation integration over several pings, which are not discussed here.

The method first beamforms the physical sonar array for an initial value of ρ_p using time-domain backprojection and then coherently adds onto the current SAS image. For $p > 1$, ρ_{p-1} is used as an initial point in the search with bounds $[v_\ell \dots v_u]$ that depend on the differential sway $d\rho = \rho_p - \rho_{p-1}$. The bounds are measured in fractions of wavelengths, with a large $d\rho$ resulting in wider bounds, from a minimum of $\lambda/2$ up to a maximum of 6λ. Initially, the INS sway is used as a starting point and a large search area is required to correct for large sway offsets, after which the bounds begin to converge to their minimum values. This is based on a smoothness assumption for the ping-to-ping sway, which is not unreasonable for the large UUV platform used in this paper. Jumps of $\lambda/2$ are also unwrapped to preserve this smoothness: since the resolution cell (roughly 1.5 cm) is larger than the wavelength, it is not possible to distinguish between sways $\lambda/2$ apart (corresponding to a two-way travel time of λ, or a 2π phase shift). An exhaustive search over $[v_\ell \dots v_u]$ must be performed if one is to search over a range that is greater than $\lambda/2$. Of course, if one could guarantee that bulk sway has been compensated then a traditional gradient descent method could be applied in order to speed up computation time; this was not done here. An important consideration is that only sway is computed here as the INS yaw and surge were found to be sufficiently accurate to focus the images. It is easy yet computationally expensive to modify this method to optimize these other parameters.

2.2 Results on downward-facing SAS data

The method was first tested and compared to the traditional DPCA method using data collected in 2013 in the Bedford Basin near Halifax, Nova Scotia using the Kraken Aquapix INSAS2 system mounted on-board of the Arctic Explorer UUV (described below). Large areas of the seafloor were systematically surveyed to collect data for scientific analysis and signal processing development. The image is shown in Figure 1 and contains an area of speckled, featureless seafloor as well as a large shipwreck and a small object, likely a rock, nearby. The first image (left panel) shows the results of using only the INS sway in focusing the images. The image clearly shows the along-track blurring and repeated copies of strong scatterers that is typical in images with uncompensated sway. The second image (middle panel) is one created using DPCA, showing a higher image quality, as expected, and the change in shadow definition can be most clearly observed in the small object. Finally, the third image (right panel) was created by using the proposed sharpness optimization method. Qualitatively, it appears to better focus small point scatterer and provide greater shadow definition. A comparison of the DPCA-derived and autofocus-derived sway is shown in Figure 2. DPCA processing is performed over range windows (in this case four) with different sway and surge estimates used in each. The four windows with central ranges of 36, 41, 49 and 60 meters are shown with the DPCA sway given in the solid grey line and the sharpness-optimized sway with black dots which show good agreement with the DPCA method. In the case of the third range window, the sway is offset by a factor of $\lambda/2$ (the dotted line shows this line); as already mentioned, since the resolution of the image is greater than λ, these 2π phase shifts cannot be separated, however it does not have an effect on the resulting image.

3 ANALYSIS

In order to analyse the autofocus method, target data without the seabed was collected as part of the PISCES3 experiment (Program for an Interferometric SAS on a Canadian Experimental System); this was the third in a series of experiments conceived to develop and test UUV-based HF SAS systems. The data considered here contained four simple (either cylindrical or spherical) objects deployed in a line at different depths below the surface collected using a UUV equipped with an upward looking MINSAS system, which is variation of the INSAS2 designed for integration into smaller platforms. The system is essentially identical to the INSAS2 including frequency and bandwidth.

The data was collected during the last weeks of March and beginning of April 2014 in the Bedford Basin. Historical data for this period obtained from Environment Canada[2] shows wind speeds of roughly 5 knots in the morning, increasing to 10 knots in the early afternoon, with a correspondingly low sea

[2] http://climate.weather.gc.ca/

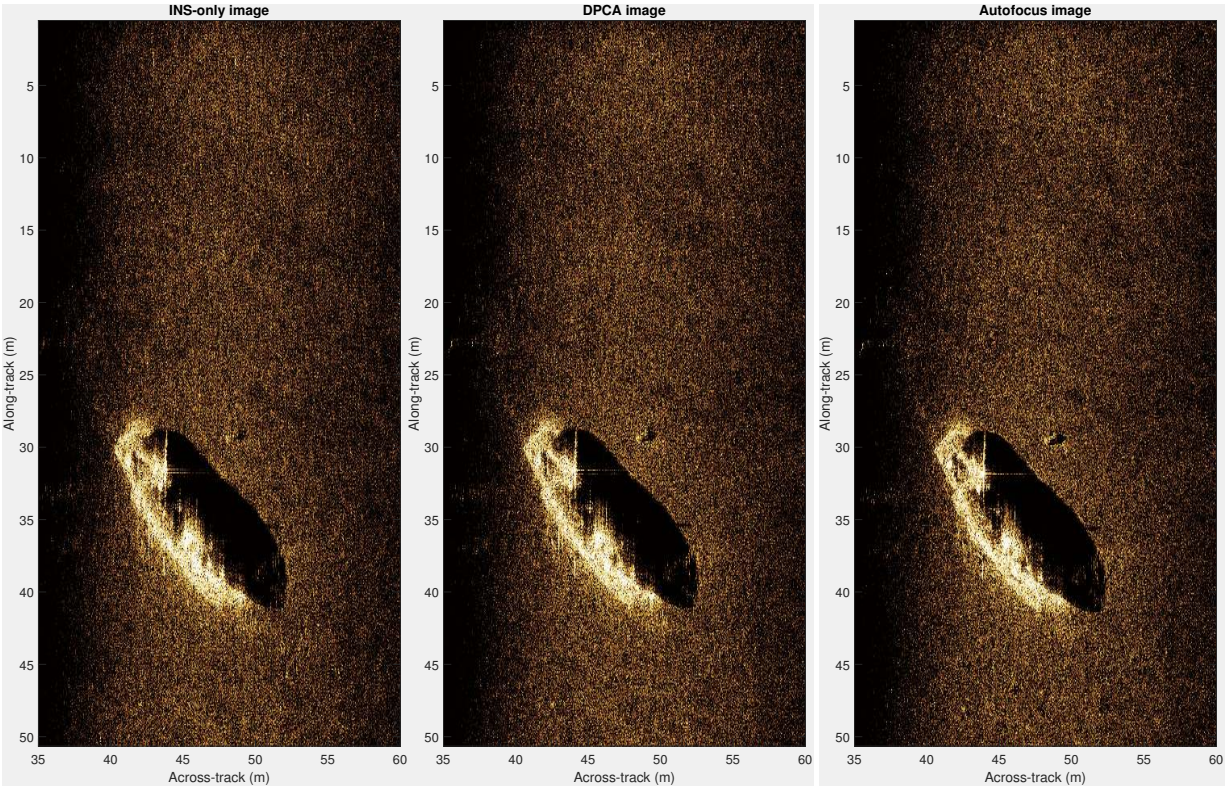

Figure 1: SAS image created using backprojection with INS-only, DPCA and autofocus-derived sway estimates shown from left to right.

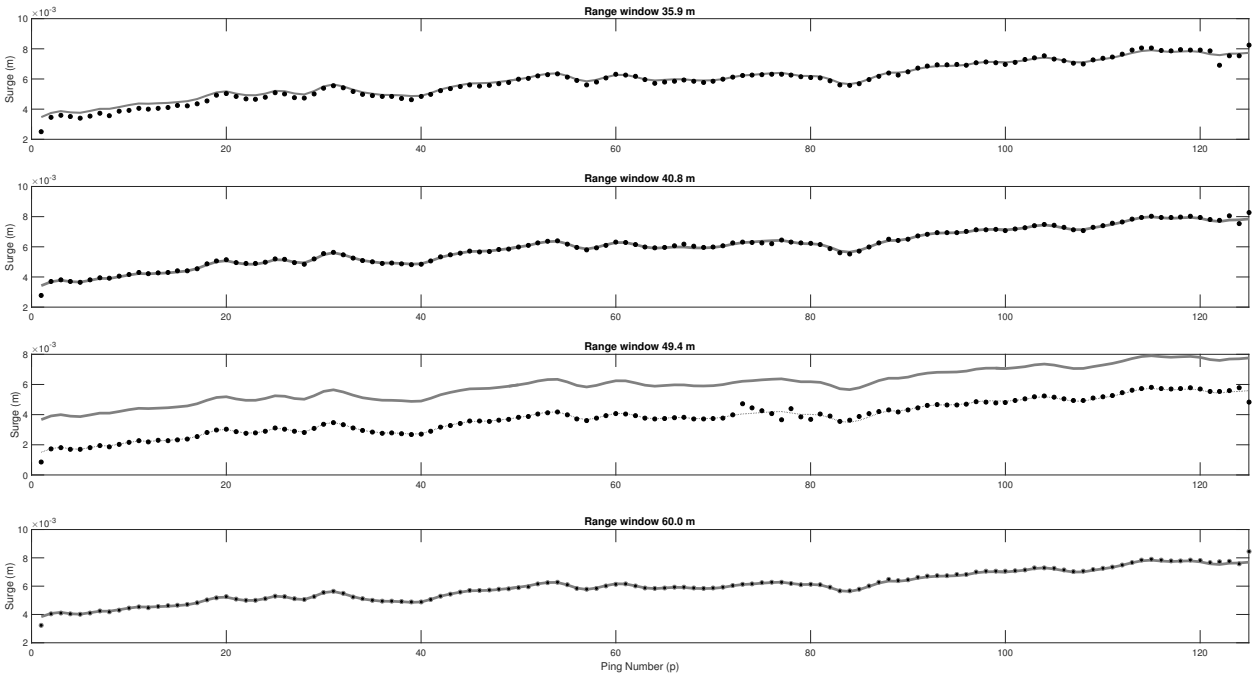

Figure 2: Comparison of DPCA (solid line) and autofocused (dots) sway tracking.

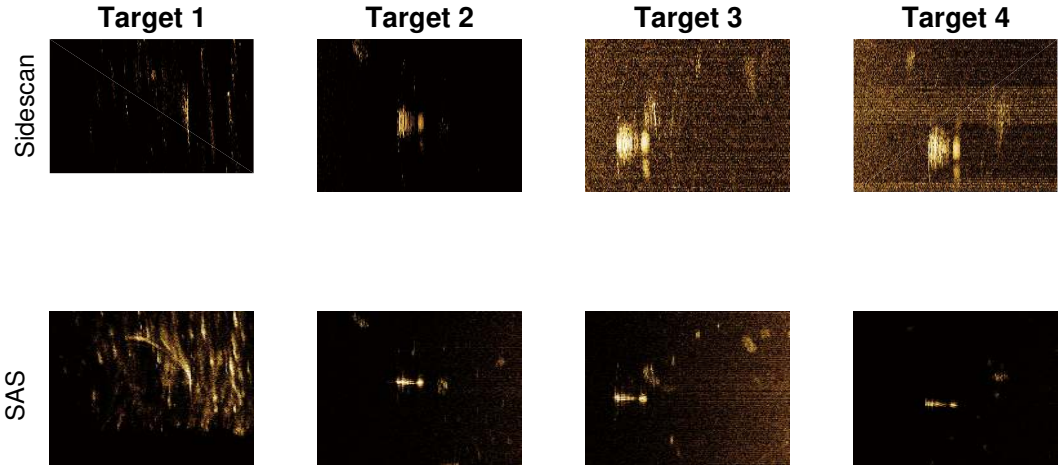

Figure 3: Zoomed in focused sidescan (top) and autofocused SAS (bottom) images of the deployed targets for run 1. All images have a 50 dB of dynamic range.

state for the initial part of the day, with some small crests and scattered white caps forming by the late afternoon. The UUV was programmed to survey the targets on the starboard side in a racetrack pattern and at different ranges.

The autofocus method is applied in order to create focused SAS images of the deployed objects which are then compared to images created using dynamic focusing beamforming techniques, where for each ping, all of the receive transducers are used to create an image which is stacked with previous pings. This results in "waterfall" image of the type commonly seen in sidescan sonar displays.

A key difference is that multi-element real-aperture sidescan sonar are usually designed to have a narrow transmit beamwidth in order to increase the radiometric resolution of the images. SAS systems, on the other hand, are designed to have wide transmit beamwidth in order to increase the length of the synthetic array[3]. Imagery obtained from one of the four runs in the data is presented in Figure 3 showing both sidescan and SAS processing. Only images of the deployed objects are given. The depth for each of the runs was approximately 37 m while the altitude from the seafloor was nominally 28 m. The maximum range setting for the sonar based on the platform speed and pulse repetition interval was 225 m, and the length of each run was approximately 400 m. As is commonly done in most dynamically focused sidescan systems, areas of overlap between pings are marked as redundant and not displayed in order to create an image that is as free of distortions as possible. In this particular run, the objects are imaged at relatively short range. The SAS processing has significantly improved the resolution of the images in all the cases, and the autofocus method has succeeded in focusing the object images. The coherent summing of multiple pings has also improved the Signal to Reverberation Ratio (SRR) of the SAS images. This is expected as the returns from the stationary targets are summed coherently and increases the SRR [9].

A closer examination of the objects shows some blurring artefacts, perhaps caused by movement of the objects during the sonar imaging process. The deepest deployed object (labelled Target 1 in Figure 3) appears similar in the imagery for all runs, regardless of range and depth of the platform, but exhibits much different characteristics than the other objects, even in the sidescan images. It is unclear as to why this should be the case, although it could be due to a number of reasons including an incorrect deployment.

[3]A well-known relation in synthetic aperture imaging systems is that the achievable resolution is proportional to total integration angle, defined by the beamwidth.

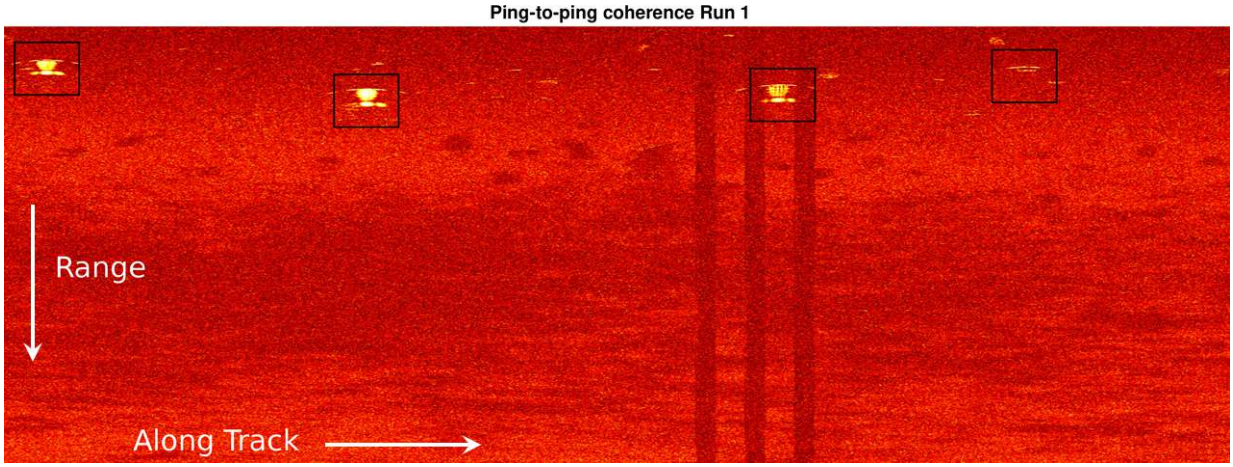

Figure 4: Ping-to-ping coherence for Run 1, with the target locations highlighted. Colours show coherence between 0 (dark red) and 1 (white).

3.1 Ping-to-ping coherence

It is interesting to examine the ping-to-ping coherence of the SAS throughout the run. Here is it used to analyse the coherence of the objects and surface between successive pings as a potential performance metric. The sample ping-to-ping (magnitude) coherence two signals s_p and s_{p+1} using k measurements within a window centred at range r is:

$$\gamma_{p2p} = \left| \frac{\sum_k s_p(r) s_{p+1}(r)^*}{\sqrt{\sum_k |s_p(r)|^2} \sqrt{\sum_k |s_{p+1}(r)|^2}} \right|, \tag{7}$$

this is a measure of similarity between p and $p+1$ at the given range. The ping-to-ping coherence γ_{p2p} for a window size 1.5 m for run 1 is shown in Figure 4. In this example, the three shorter range objects are clearly observable. When the ping-to-ping coherence is high it provides a reliable way of observing the objects even in the presence of high reverberation. As expected, the sea surface itself is not coherent (but not 0, partially due to the bias of the sample coherence [16]) and DPCA methods would not be expected to provide acceptable performance [4].

4 CONCLUSION

This paper has presented initial results from a new autofocus method which uses a sharpness based criterion for creating focused SAS imagery. The method has been tested, firstly on downward facing SAS where it was compared with DPCA where it was found to produce similar results, and then for a very poor DPCA performance situation (a surface-facing SAS) where it has been shown to improve the focusing for objects below the sea surface. It is perhaps not surprising that a coherence maximization method (like DPCA) and sharpness maximization method should produce similar results. It has been shown in optics that sharpness and coherence are equivalent [10] , however, to our knowledge, a similar relation has not been shown for the case of narrow band sonar. While the present method shows some advantages over DPCA, it is unlikely to replace it as a primary method for SAS motion compensation in a practical SAS system. The computational efficiency and elegance of the DPCA method will continue to make it the primary choice for SAS micronavigation solutions, and applying a more traditional post-micronavigation statistical autofocus method, such as the ones discussed above, will likely provide similar image quality without the computational expense. While the object imagery has been improved through SAS processing, it is unclear as to why the focus of the objects in the SAS images is not as sharp

[4] It must be pointed out that one could apply DPCA micronavigation to only the targets, since they exhibit some coherence from ping-to-ping at short and medium ranges.

as in downward-facing systems. Strong side lobes were observed, especially at short ranges. This is possibly due to the undersampling of the array due to some technical challenges that occurred during the data collection, but could also be attributed to the movement of the objects through the duration of the illumination.

ACKNOWLEDGEMENTS

The authors would like to thank Kraken Robotics and Atlas Elektronik UK for their effort in executing the data collection effort during the PISCES3 trial, in particular Sean Chapman and David Shea, as well as the Fleet Diving Unit (Atlantic) for the deployment and recovery of the objects.

References

[1] J. N. Ash, "An autofocus method for backprojection imagery in synthetic aperture radar," *IEEE Geoscience and Remote Sensing Letters*, vol. 9, no. 1, pp. 104–108, Jan 2012.

[2] M. Born and E. Wolf, *Principles of Optics*, 7th ed. Cambridge University Press, 1999.

[3] H. Callow, M. Hayes, and P. Gough, "Stripmap phase gradient autofocus," in *Proceedings of OCEANS 2003*, vol. 5, Sept 2003, pp. 2414–2421.

[4] W. Carrara, R. Goodman, and R. Majewski, *Spotlight Synthetic Aperture Radar*. Artech House, 1995.

[5] D. Cook and D. Brown, "Analysis of phase error effects on stripmap SAS," *IEEE Journal of Oceanic Engineering,*, vol. 34, no. 3, pp. 250–261, July 2009.

[6] F. R. Dickey, M. Labitt, and F. M. Staudaher, "Development of airborne moving target radar for long range surveillance," *IEEE Transactions on Aerospace and Electronic Systems*, vol. 27, no. 6, pp. 959–972, Nov 1991.

[7] J. R. Fienup, "Synthetic-aperture radar autofocus by maximizing sharpness," *Optics Letters*, vol. 25, no. 4, pp. 221–223, Feb 2000. [Online]. Available: http://ol.osa.org/abstract.cfm?URI=ol-25-4-221

[8] S. Fortune, M. Hayes, and P. Gough, "Statistical autofocus of synthetic aperture sonar images using image contrast optimisation," in *OCEANS, 2001. MTS/IEEE Conference and Exhibition*, vol. 1, 2001, pp. 163–169.

[9] J. Groen, M. Couillard, and W. Fox, "Synthetic aperture sonar array gain measured at sea," in *European Conference on Synthetic Aperture Radar*, 2012, pp. 74–77.

[10] J. P. Hamaker, J. D. O'Sullivan, and J. E. Noordam, "Image sharpness, Fourier optics, and redundant-spacing interferometry," *J. Opt. Soc. Am.*, vol. 67, no. 8, pp. 1122–1123, Aug 1977. [Online]. Available: http://www.osapublishing.org/abstract.cfm?URI=josa-67-8-1122

[11] R. Hansen, *Introduction to Synthetic Aperture Sonar*. InTech, 2011.

[12] R. Heremans, M. Acheroy, and Y. Dupont, "Motion compensation on synthetic aperture sonar images," in *2006 IEEE Ultrasonics Symposium*, Oct 2006, pp. 152–155.

[13] J. Kolman, "PACE: An autofocus algorithm for SAR," in *IEEE International Radar Conference*. IEEE, 2005, pp. 310–314.

[14] T. Marston and D. Plotnick, "Semiparametric statistical stripmap synthetic aperture autofocusing," *IEEE Transactions on Geoscience and Remote Sensing*, vol. 53, no. 4, pp. 2086–2095, April 2015.

[15] M. Pinto, "High resolution seafloor imaging with synthetic aperture sonar," *Oceanic Engineering Newsletter*, pp. 15–20, 2002.

[16] R. Touzi, A. Lopes, J. Bruniquel, and P. W. Vachon, "Coherence estimation for SAR imagery," *IEEE Transactions on Geoscience and Remote Sensing*, vol. 37, no. 1, pp. 135–449, 1999.

[17] D. E. Wahl, P. H. Eichel, D. C. Ghiglia, and C. V. Jakowatz, "Phase gradient autofocus-a robust tool for high resolution SAR phase correction," *IEEE Transactions on Aerospace and Electronic Systems*, vol. 30, no. 3, pp. 827–835, Jul 1994.